Energy Fuels **XXXX,** *XXX,* 000–000 · DOI:10.1021/ef900348h

energy&fuels
article

Morphological Characteristics of Gold Nanowires and Nanoparticles: Structure Elucidation and Reactivity Toward Water-gas Shift Reaction

Mohamed Mokhtar Mohamed*,† and K. S. Khairou‡

†*Department of Chemistry, Faculty of Science, Benha University, Benha, Egypt, and* ‡*Department of Chemistry, College of Applied Science, Umm Al-Qura University, Makah, Saudi Arabia*

Received April 28, 2009. Revised Manuscript Received July 10, 2009

Irradiation of γ-ray to FSM-16 encapsulated $HAuCl_4$, synthesized via chemical vapor deposition, led to the formation of Au nanowires (2−10 nm diameter and 17−147 nm length). Contrarily, reductive carbonylation of impregnated $HAuCl_4$ with FSM-16 using CO (200 torr)/water (20 torr) for 2 h, followed by irradiation with a high-pressure Hg lamp at 300 K for 36 h, resulted in the formation of Au nanoparticles (circular; 8−75 nm diameter). These catalysts have been characterized by XRD, N_2-sorpitometry, TEM, UV−vis-DRS, CO-FTIR spectroscopy, and then tested for water-gas shift reaction (WGSR) under feeding conditions of $P_{CO} = 60$ torr and $P_{H_2O} = 5$ torr. Evidently, Au nanowires exhibited higher activity (3 times) than Au nanoparticles. It has been shown that the activity depends on Au geometry rather than structural characteristics, such as surface area. In-situ FTIR CO adsorption and UV−vis-DRS evidenced major changes on the surface properties of Au nanowires in exposing different oxidation states as well as inducing electron deficiencies exceeding those on Au nanoparticles. Gold nanowires displayed a surface plasmon resonance peak at 525 nm derivatized from distribution in size and dispersion and rather exceeding that at 484 nm exhibited for gold nanoparticles. It has been shown that Au^0 species, including nanowires and small aggregated metallic nanoparticles, contribute significantly, if not predominantly, to the WGS activity. The TEM study provided evidence that reduction pretreatment of Au nanowires prior to carrying out the reaction results in elimination of the activity due to sintering (from 35 to 53 nm) as well as to the exhibited change in geometry and thus altering the nature of active centers.

1. Introduction

Noble metal nanoparticles, and in particular gold, are interesting materials for many applications including catalysis, optics, and electronics[1,2]. Intense effort has been dedicated to controlling the size, shape, and structural architectures of nanocrystals through manipulation induced by various techniques. To date, many gold nanostructures, such as wires[3], rods[4], plates,[5−11] cubes and boxes[12], triangles[13], and branched structures[14,15] have been synthesized. Gold exhibits a unique catalytic nature and action when it is deposited as nanoparticles on a variety of metal oxides.

The new generation of mesoporous materials is increasingly being used in various commercial catalysts because of their high surface area, unique pore sizes, thermal stability, etc. Mesoporous silica such as FSM-16[16,17] has been used as templates to synthesize free-standing nanoplatinum wires fabricated by CO (200 torr)/water (20 torr) under a high-pressure Hg lamp at 300 K, induced from impregnation with H_2PtCl_6.[18,19] It has been shown that the catalysis of the Pt nanowires in comparison with nanoparticles toward water-gas shift reaction was superior. Nanoparticles and short nanowires of Au are also synthesized in mesoporous thin films.[20] Other groups also reported that the Pt nanowires were formed by H_2-reduction of Pt ions in the channels of MCM-41.[21,22] Recently, Haruta have revealed that the catalytic performance of supported gold catalysts markedly depends

*To whom correspondence should be addressed. E-mail: mohmok2000@yahoo.com.

(1) El-Sayed, M. A. *Acc. Chem. Res.* **2002**, *34*, 257.
(2) Burda, C.; Chen, X. B.; Narayanan, R.; El-Sayed, M. A. *Chem. Rev.* **2005**, *105*, 1025.
(3) Kim, J. U.; Cha, S. H.; Shin, K.; Jho, J. Y.; Lee, J. C. *Adv. Mater.* **2004**, *16*, 459.
(4) Murphy, C. J.; Sau, T. K.; Gole, A.; Orendorff, C. J. *MRS Bull.* **2005**, *30*, 349.
(5) Tsuji, M.; Hashimoto, M.; Nishizawa, Y.; Tsuji, T. *Chem. Lett.* **2003**, *32*, 1114.
(6) Wang, L. Y.; Chen, X.; Zhan, J.; Sui, Z. M.; Zhao, J. K.; Sun, Z. W. *Chem. Lett.* **2004**, *33*, 720.
(7) Sun, X. P.; Dong, S. J.; Wang, E. K. *Angew. Chem., Int. Ed.* **2004**, *43*, 6360.
(8) Sun, X. P.; Dong, S. J.; Wang, E. K. *Langmuir* **2005**, *21*, 4710.
(9) Wang, L. Y.; Chen, X.; Zhan, J.; Chai, Y. C.; Yang, C. J.; Xu, L. M.; Zhuang, W. C.; Jing, B. *J. Phys. Chem. B* **2005**, *109*, 3189.
(10) Li, Z. H.; Liu, Z. M.; Zhang, J. L.; Han, B. X.; Du, J. M.; Gao, Y. N.; Jiang, T. *J. Phys. Chem. B* **2005**, *109*, 14445.
(11) Kawasaki, H.; Yonezawa, T.; Nishimura, K.; Arakawa, R. *Chem. Lett.* **2007**, *36*, 1038.
(12) Sun, Y. G.; Xia, Y. N. *Science* **2002**, *298*, 2176.
(13) Keribig, U.; Vollmer, M. *Optical Properties of Metal Clusters*; Spriger: Berlin, 1995.
(14) Guo, S. J.; Wang, Y. L.; Wang, E. K. *Nanotechnology* **2007**, *18*, 405602.
(15) Li, Z. G.; Friedrich, A.; Taubert, A. *J. Mater. Chem.* **2008**, *18*, 1008.
(16) Mohamed, M. M.; Eissa, N. A. *Mater. Res. Bull.* **2003**, *38*, 1993.
(17) Mohamed, M. M.; Mekkay, I. *J. Phys. Chem. Solids* **2003**, *64*, 299.
(18) Mohamed, M. M.; Thabet, M. J. *Phys. Chem. C* **2008**, *112* (24), 8890.
(19) Sasaki, M.; Osada, M.; Higashimoto, N.; Yamamoto, T.; Fukuoka, A.; Ichikawa, M. J. *Mol. Catal. A* **1999**, *141*, 223.
(20) Fukuoka, A.; Araki, H.; Sakamoto, Y.; Sugimoto, N.; Tsukada, H.; Kumai, Y.; Akimoto, Y.; Ichikawa, M. *Nano Lett.* **2002**, *2*, 793.
(21) Ko, C. K.; Ryoo, R. J. *Chem. Soc., Chem. Commun.* **1996**, 2467.
(22) Liu, Z.; Sakamoto, Y.; Ohsuna, T.; Hiraga, K.; Terasaki, O.; Ko, C. H.; Shin, H. J.; Ryoo, R. *Angew. Chem., Int. Ed.* **2000**, *39*, 3107.

©XXXX American Chemical Society

on the degree of dispersion, support, and preparation methods.[23] The supported Au nanoparticles show high catalytic activities in reactions such as CO oxidation and oxidation−decomposition of amines and organic halides. It was also reported that nanostructured Au metal with rod-like structure was formed on MCM-41, and their catalytic performance in CO oxidation was investigated.[24] Au nanowires with a diameter of 7 nm were also prepared in the mesopores of SBA-15.[25] The catalytic properties of these materials largely depend upon the Si/Al ratio, degree of cation exchange, extra-framework element, surface treatment, etc.[26,27]

However, the preparation of silica-supported gold nanoparticles with high activity remains a challenge because of the limitation of the isoelectric point of silica. To make highly active gold catalysts, sol−gel[23,28] and microemulsion[29] methods have been developed; however, the dispersion and size distribution of gold nanoparticles on silica are far from satisfactory. The relationship between catalytic activity and particle size has already been claimed in the literature[30,31] and some other effects such as the metal−support interaction and the oxidation state of gold have in turn been considered as determining factors for many reactions. On the basis of the limited role played by mesoporous silica as noninteracting oxide toward gold, that is, negligible metal−support interaction, we try to investigate the influence of morphology (shape and size) of gold nanoparticles on their catalytic performances toward water-gas shift reaction. That is an important reaction in a number of chemical processes for the production of H_2. Thus, we present a novel selective synthesis of Au nanowires in the mesopores of FSM-16 through irradiating the encapsulated tetrachloroauric acid, of high vapor pressure—synthesized via chemical vapor deposition technique—by gamma ray. The catalytic activity of nanowires was compared with those of nanoparticles; prepared by reductive carbonylation, of impregnated $HAuCl_4$, via CO/H_2O mixture. By using various characterization methods; including XRD, N_2 adsorption, UV−vis diffuse reflectance, TEM, and in situ FTIR of CO adsorption, it is possible to put forward plausible explanations for the observed differences in catalytic performances.

2. Experimental Section

2.1. Sample Preparation. FSM-16 was prepared according to the published procedures.[16] The BET surface area was 1015 $m^2 g^{-1}$, and the pore size was 2.93 nm. The powdered sample of FSM-16 was dried under vacuum (ca. 10^{-4} torr, 1 torr = 133 Pa) at 623 K for 2 h. Five weight percent Au/FSM-16 was prepared at room temperature by careful mixing of tetrachloroauric acid ($HAuCl_4 \cdot 3H_2O$, Strem chemical) with dried FSM-16 under a nitrogen atmosphere in a Schlenk-like tube that was left overnight under stirring for assuring complete mixing. Then, this tube was fixed in a homemade vacuum system under reduced (10^{-4} torr) pressure at 338 K for 24 h, allowing the vapor of $HAuCl_4$ to diffuse into the pores of silica. This material was then irradiated using cobalt-60 irradiator with the activity of 2000 curie at a dose of 2.5×10^5 rads/h for 6 h. This sample produced gold nanowires that were referred to as AuFSwire.

Other Au/FSM-16 sample (5 wt % Au) was prepared by the impregnation method as follows. On the FSM-16 slurry, a slow addition of an aqueous solution of $HAuCl_4$ with rapid stirring continued for 8 h at 300 K was obtained and then transferred to a rotary evaporator that works at 340 K and finally vacuum-dried (10^{-4} torr) at the same temperature. This sample, which was charged in a quartz cell ($15 \times 15 \times 1.5$ mm) and exposed to CO (200 torr)/water (20 torr) for 2 h, was then irradiated at 300 K by a high-pressure Hg lamp for 36 h [(F18W-BLB) $\lambda > 254$ nm] with a water jacket to avoid external heating, and formed gold nanoparticles that were referred to as AuFSpart.

2.2. Sample Characterization. *2.2.1. X-ray Diffraction.* The X-ray powder diffraction (XRD) patterns of various solids were carried out using a Philips 321/00 instrument. The patterns were run with Ni-filtered Cu Kα radiation ($\lambda = 1.541$ Å) at 36 kV and 16 mA with scanning speed of 2° in 2θ min^{-1}. The XRD phases present in the samples were identified with the help of ASTM powder data files.

2.2.2. N_2 Adsorption. The surface properties, namely, BET surface area, total pore volume (Vp), and mean pore radius (r) were determined from N_2 adsorption isotherms measured at 77 K using conventional volumetric apparatus. The samples were outgassed at 473 K for 3 h under a reduced pressure of 10^{-5} torr before starting the measurement. The total pore volume was taken from the desorption branch of the isotherm at $p/p^0 = 0.95$, assuming complete pore saturation.

2.2.3. UV−vis Diffuse Reflectance Spectroscopy. UV−vis diffuse reflectance spectra of various samples in the 700−300 nm range were obtained using a Jasco V-570 (serial number, C 29635) spectrophotometer, which is attached to a diffuse reflectance accessory.

2.2.4. In Situ FTIR. In situ FTIR spectra of the samples were carried out in a closed circulation system with a dead volume of 168 cm^3. An IR cell equipped with NaCl windows was used for pretreatment and measurements. A self-supported wafer (20 mg) was prepared under nitrogen atmosphere and mounted to the sample holder in the IR cell. The wafer was evacuated at the desired temperature for 30 min before CO (20 torr) adsorption at room temperature. The IR spectra were recorded with a resolution of 2 cm^{-1} using a Jasco double beam FTIR-40.

2.2.5. Transmission Electron Microscope (TEM. TEM micrographs were measured using a Philips, model Tecani Feil2, at an accelerating voltage of 200 KV. The powder samples were put on carbon foil with a microgrid. TEM images were observed with minimum electron irradiation to prevent damage to the sample structure.

2.2.6. Catalytic Reaction. The catalytic performances in the water-gas shift reaction (WGSR) were studied using a closed circulation system with a Pyrex-glass U-type reactor, which was charged with 100 mg of catalysts. The WGSR proceeded at 323 K and 60 torr for CO and at 5 torr for H_2O. The catalysts were treated by heating the samples under vacuum (10^{-4}) at 323 K for 0.5 h prior to the admission of the reacting gas mixture. The gas phase reactants and products were analyzed by online gas chromatography (Shimadzu-14C), using Porapak q and molecular sieve 13X, with a thermal conductivity detector operated at 60 °C for the separation of CO, CO_2, and H_2.

3. Results and Discussion

3.1. TEM and XRD Investigations. As presented in Figure 1, the TEM image showed that nanostructured Au wires [2−10 nm diameter and 17−147 nm length; with a mean length of 58 nm] were formed in alignment along the

(23) Haruta, M. *Catal. Today* **1997**, *36*, 153.
(24) Okumura, M.; Tsubota, S.; Iwamoto, M.; Haruta, M. *Chem. Lett.* **1998**, 315.
(25) Han, Y. J.; Kim, J. M.; Stucky, G. D. *Chem. Mater.* **2000**, *12*, 2068.
(26) Mohamed, M. M.; Salama, T. M.; Ohnishi, R.; Ichikawa, M. *Langmuir* **2001**, *17*, 5684.
(27) Jeon, J. Y.; Kim, H. Y.; Woo, I. S. *Appl. Catal. B: Environ.* **2003**, *44* (4), 301.
(28) Gupta, N. M.; Tripathi, A. K. *J. Catal.* **1999**, *187*, 343.
(29) Walker, C. H.; John, J. V.St.; Neilson, P. W. *J. Am. Chem. Soc.* **2001**, *123*, 3846.
(30) Sacaliuc-Parvulescu, E.; Friedrich, H.; Palkovits, R.; Weckhuyen, B. M.; Nijhuis, T. A. *J. Catal.* **2008**, *259*, 43.
(31) Akolekar, D. B.; Bhargava, S. K. J. *Mol. Catal.* **2005**, *236*, 77.

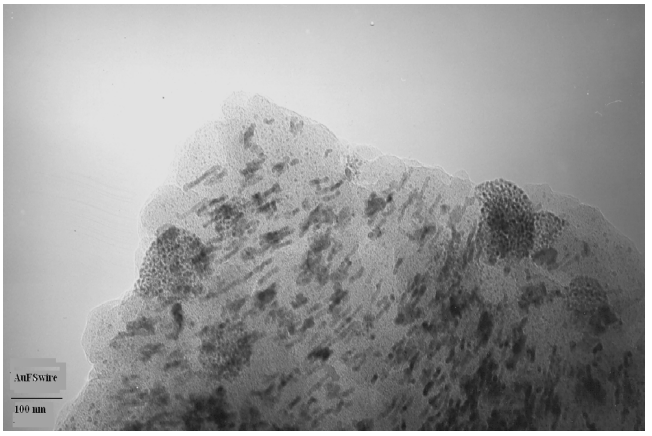

Figure 1. TEM image of Au-nanowires obtained following exposure of $HAuCl_4$ encapsulated in FSM-16, and synthesized by CVD method, to γ-rays at 300 K.

channels of the FSM-16 (2.93 nm) host. Increasing the mean diameter of this sample (4.3 nm) compared to that of the host proposes the presence of major parts of nanowires on the external surfaces of the mesoporous channels and thus, a significant loss in surface area is expected (see Table 1). The presence of distinctive aggregates of spherical Au nanoparticles in the size of 2−11 nm, specifically at both sides of the image, evidence that the formation of nanowires was originally resulted from nanoparticles and thus highlighting the incomplete transformation of the nanoparticles. One can easily manipulate TEM to observe only nanowires irrespective of nanoparticles; however, distinguishing detectable amounts of nanoparticles can not be ignored. Accordingly, multiple shots of TEM images indicate higher population percentage for the wire (75%) shape exceeding those of nanoparticles ones (25%). TEM results presented in Figure 2 showed that Au nanoparticles of 8−75 nm diameters were formed; with a mean equivalent to 35 nm, and indeed to some extent occupy major parts of the FSM-16 external surface. These atoms were not uniformly distributed along the ordered mesoporous channels of FSM-16 crystals, that is, they are prone to aggregation, with significant formation of external particles.

XRD diffractograms of Au/FSM-16 catalysts in the 1.5−70° range are shown in Figure 3. The XRD pattern of the as prepared AuFSpart sample gives evidence of the presence of very narrowed diffraction peaks due to the face-centered cubic (fcc) structure of gold at *d*-spacings equal to 2.36 (111), 2.04 (200), and 1.44 (220) Å, characterizing metallic gold species;[32] whereas it can hardly be detected on AuFSwire sample, indicating that the average particle size was too small to be detected by XRD, that is, gold wires were highly dispersed. A rough estimate of gold particle size, for AuFSpart, by the Scherrer approximation results in Au clusters within average diameter of 30 nm, which is comparable to those obtained from TEM results. Maintaining the Au diffraction for this sample, unlike the case in nanowires, is most likely due to the large Au particles that possess the requisite long-range order required for diffraction. The XRD analyses also suggest that Au nanoparticles were more developed along the ⟨111⟩ direction, forming a raft-type structure. AuFSpart also shows distinct humps at Bragg angles (2θ) of the 10−30° range together with well-developed peaks at 2 and 4°, those matches with the topology of FSM-16 structure.[16] These humps (peaks), except the one at $2\theta = 2°$, were faded on AuFSwire probably due to dispersion of Au nanowires and to the strong interaction offered between Au and silica, particularly in this sample. Maintaining XRD lines of FSM-16 at low angles for both samples[33] indicates the conservation of their pore structures even following the formation of nanowires and nanoparticles. When the gold nanoparticles are synthesized by the conventional chemical reduction method, the gold atoms are packed with the fcc mode exposing ⟨111⟩ planes, spontaneously resulting into the formation of spherical shape.[34]

3.2. N_2 Sorption Measurements. Nitrogen isotherms of calcined AuFS samples given in Figure 4 exhibit type IV isotherms with clear adsorption−desorption hysteresis loops, which are characteristics of large pore mesoporous materials with cylindrical pores. It can be seen that the mesopore system of AuFSwire differs very much from that in AuFSpart not only the mesopore volume is larger (see also Table 1) for the wire sample but also the shape of the hysteresis loop is very different. At a relative pressure of ca. 0.45 for AuFSwire, there is a sudden desorption of nitrogen, which is visible as about to close of the hysteresis loop at this pressure but however extended widely again to meet at relative pressure near to zero, indicating the existence of two types of pores. This manifests the appreciable change in the size distribution of the nanowires. For AuFSpart, the hysteresis loop shows desorption and closing point at P/P^0 equals 0.3, indicative of the presence of a wide range of mesopores.

The micropore volume of the FSM-16 containing nanowires was lower than that of the one enclosing nanoparticles due to blocking of these pores by gold nanowires. The large diameter of the nanowire structure leads to its coincidence with the cylindrical mesoporous channels of FSM-16; consequently, a significant loss in surface area (25.3%) was depicted, whereas AuFSpart exhibited a lower decrease (15.8%). This indicates that the wires might extended throughout the pore diameter of the host FSM-16 (Table 1), however a slight increase in pore radius (31.3 Å) was depicted, suggesting well entrapping and enforcing of Au nanowires deep inside the pore volume. This proposes that interconnection of cylindrical mesopores could have occurred.[35] Conversely, AuFSpart showed a marked decrease in the pore radius into 20.51 Å due to occupation of the FSM-16 channels and outer surfaces by Au nanoparticles, as emphasized from XRD and TEM results that demonstrated the presence of large particles of Au^0 species.

More emphasis into the pore type and its influence by the structure of Au nano can be imposed from V_l-t plot (not shown). Both samples show upward deviations emphasizing again the existence of mesopores. The plot of AuFSpart possessed a texture dominated by wider pores; in the 6.0−12.5 Å range; as assessed previously by hysteresis loop, than AuFSwire; 4.5−10.0 Å, which showed lower S_{BET} comparatively. Although the texture of the later sample was dominated by narrower pores than those presented by AuFSpart,

(32) Salama, T. M.; Shido, T.; Ohnishi, R.; Ichikawa, M. *J. Phys. Chem.* **1996**, *100*, 3688.

(33) Araki, H.; Fukuoka, A.; Sakamoto, Y.; Inagaki, S.; Sugimoto, N.; Fukushima, Y.; Ichikawa, M. J. *Mol. Catal. A* **2003**, *199*, 95.

(34) Choudhary, T. V.; Goodman, D. W. *Appl. Catal., A* **2005**, *291*, 32.

(35) Janssen, A. H.; Koster, A. J.; De Jong, K. P. *J. Phys. Chem. B* **2002**, *106*, 11905.

Table 1. Surface Properties of AuFSwire and AuFSpart Encapsulated Inside the Host FSM-16, Heated at 473 K under a Reduced Pressure of 10^{-4} torr[a]

samples	S_{BET} (m^2/g)	S_t (m^2/g)	S^{ext} (m^2/g)	S^{mic} (m^2/g)	S^{meso} (m^2/g)	$V_{p_3}^{total}$ (cm^3/g)	$V_{p_3}^{mic}$ (cm^3/g)	V_p^{meso} (cm^3/g)	$\bar{r}$ (Å)	*C*-Const	microporosity %
FSM-16	1015					0.92			29.3		
AuFSpart	854	708	68	795	106	0.7395	0.6522	0.0873	20.51	38	88.2
AuFSwire	758	757	86	700	57	0.744	0.6676	0.07639	31.33	17	89.7

[a] BET surface area (S_{BET}), total pore volume (V_p), mean pore radius ($\bar{r}$), surface area derived from $V_{l\text{-}t}$ plots (S_t), surface area of micropores (S^{mic}), external surface area (S^{ext}), surface area of wide pores (S^{meso}), volume of micropores (V_p^{mic}), volume of wide pores (V_p^{meso}), and microporosity percentages.

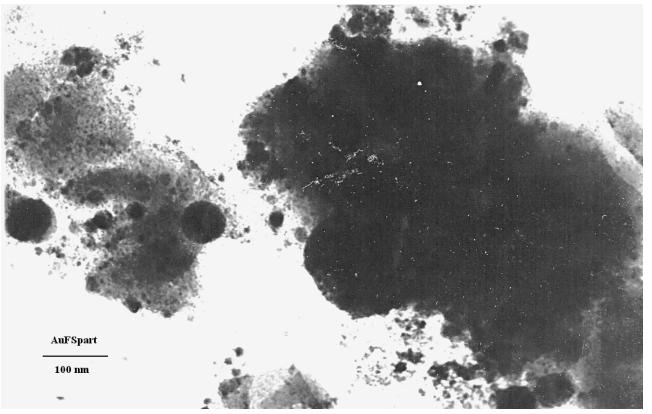

Figure 2. TEM image of Au nanoparticles obtained after exposure to CO/water (200/20 torr, 2 h) and a high-pressure Hg at 300 K.

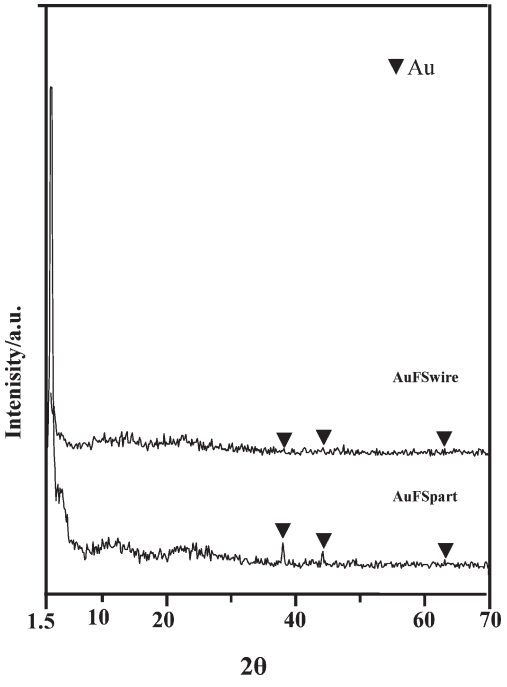

Figure 3. Powder XRD patterns of AuFSwire and AuFSpart samples.

it seems that Au nanowires find their way in narrow pores, leaving behind wider ones that were involved in decreasing the specific surface area of this particular sample.

3.3. In Situ FTIR and UV−vis Spectroscopy. CO adsorption technique provides information about the oxidation and coordination state of charge balancing cations and is widely employed for examining active sites on gold nano materials. The interaction between CO and AuFSpart and AuFSwire is

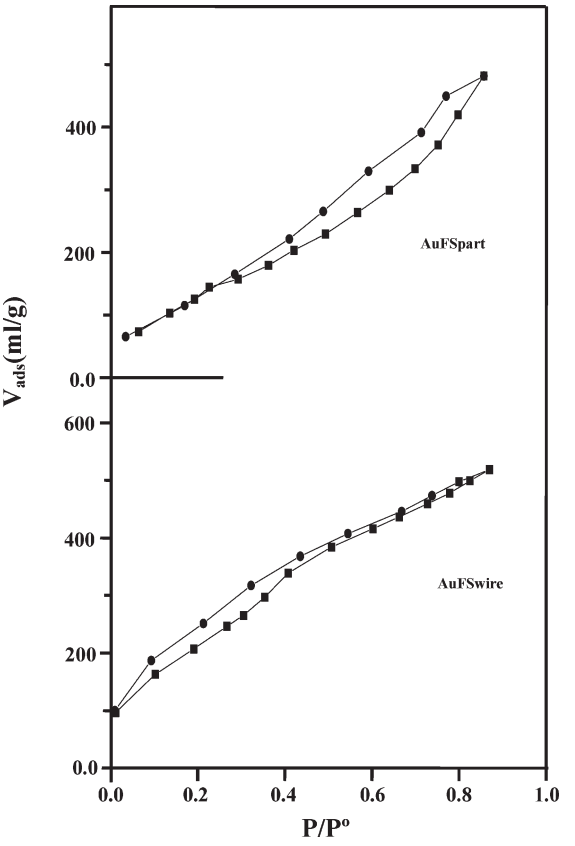

Figure 4. Adsorption−desorption isotherms of N_2 at 77 K for FSM-16 encapsulated AuFSwire and AuFSpart samples heated at 473 K.

presented in Figure 5. Following exposure to CO (22 torr at 298 K), AuFSwire produced a vibrational spectrum (a) composed of five infrared bands attributed to the CO chemisorbed on Au^+ (2178 cm^{-1}), CO adsorbed on Au metal (2122 and 2091 cm^{-1}), and bridged metal carbonyl complexes (Au−CO−Au)/negatively charged gold carbonyls (2063 and 2079 cm^{-1}).[36,37] Evacuation at 373 K (spectrum b) resulted in an evolution of a strong band at 2189 cm^{-1}, indicative of Au^{3+} sites,[38] together with the disappearance of the band at 2091 cm^{-1}. The intensity of the bands at 2122 and 2178 cm^{-1} as well as those at 2063 and 2079(2083) cm^{-1} increases, indicating the stability of these species.

FTIR CO adsorption on the AuFSpart sample showed similar types of CO species but with lower concentrations to those on the AuFSwire sample. This indicates that CO

(36) Lai, S. Y.; Qiu, Y.; Wang, S. *J. Catal.* **2006**, *237*, 303.
(37) Romero-Sarria, F.; Penkova, A.; Martinez, L. M.; Centeno, M. A.; Hadjiivanov, K.; Odriozola, J. A. *Appl. Catal., B* **2008**, *4*, 119.
(38) Mihaylov, M.; Gates, B. C.; Fierro-Gonzalez, J. C.; Hadjivanoy, K.; Knozinger, H. *J. Phys. Chem. C* **2007**, *111* (6), 2548.

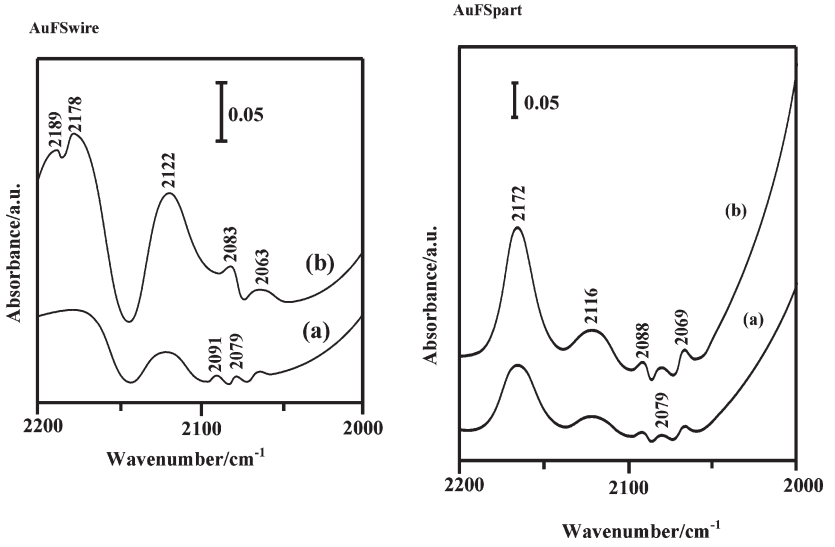

Figure 5. In-situ FTIR spectral changes of AuFSwire and AuFSpart encapsulated in FSM-16 after adsorption of 22 torr CO at 323 K as a function of time. From bottom to top after (a) 10 min and (b) evacuation at 373 K for 5 min.

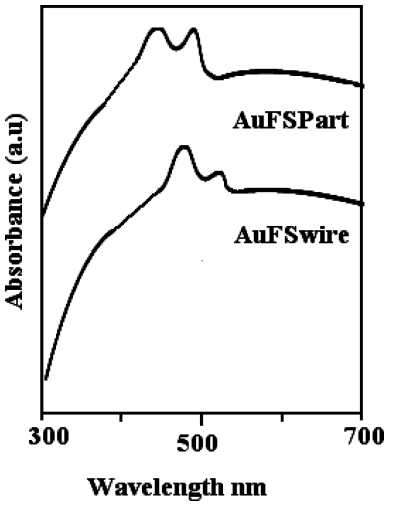

Figure 6. UV−vis diffuse reflectance spectra of Au nanoparticles (AuFSpart) and Pt nanowires (AuFSwire) encapsulated in FSM-16.

species formed on the latter were not only dominant but also more stable comparatively due to the blue shift arises for 2116 and 2172 cm^{-1} in AuFSpart into 2122 and 2178 cm^{-1} in AuFSwire. The increasing frequency shift of CO-bonded Au nanowires compared with those of Au nanoparticles gives a hint on increasing the electron deficiency, which used to be accompanied by increasing dispersion,[39] on the former comparatively, and as a result a facile reaction with CO is affirmed. Spectra of AuFSpart did not indicate the presence of Au^{3+} species. The presence or absence of Au^{3+} could be correlated with water molecules and their concentrations on the surface of silica in either promoting its existence or prohibiting it as acquired for Au nanoparticles. Provoking the oxidation of gold moieties (Au^{3+}) on the surface by water on nanowires and its negligence on nanoparticles is due to blocking of surface sites from reacting properly with CO and to what extent Au species (Au^{+}, Au^{0}) interacted with the support. Thus, one can advocate from XRD results that Au strongly bound to the support in the case of nanowires made Au^{3+} survive. Decreasing the Au−CO stretching frequency, apart from the isolated frequency of CO molecules at 2134 cm^{-1}, on gold nanoparticles (2088−2069 cm^{-1}) and on gold nanowires (2083−2063 cm^{-1}) evidence that these are formed once the two metal acquire small enough particles. From CO adsorption results, it can be seen clearly that, apart from the host support, geometrical changes of nano gold particle(wire) affected the interaction with CO molecules and thus producing different carbonyl species.

UV−vis spectroscopy was also used to verify the adsorption maxima due to the transverse surface Plasmon band of gold nano upon encapsulation inside the mesopores of silica. As can be seen in the spectra of Figure 6, absorption maxima at 475 and 525 nm were observed for AuFSwire, which were not identical to those at 445 and 484 nm depicted for AuFSpart. The presence of UV−vis absorption band at 525 nm results from Plasmon resonance on nanosized metallic wires evidence together with the discrepancy in the peak width that nanowires have distribution in size and wall thickness.[40] On the contrary, the comparable resonance band revealed for gold nanoparticles was comparatively tuned at lower wavelengths (484 nm). The intensity of the latter band was higher than that of the AuFSwire sample (525 nm), confirming the presence of smaller Au crystallites in the wire sample, as also confirmed in the XRD investigation. Increasing the absorption for gold nanowires made it promising for optical coherence tomography imaging and thus working to shift resonance peaks into the near IR is under investigation through decreasing their size distributions.

It is known that the surface plasmon resonance-wavelength observed for spherical Au nanospheres with a diameter of 20 nm is at 500 nm, which is tuned by changing their size and morphology.[41] In this study, we confirmed that the size and morphology of the gold nanoparticles can be controlled by changing the synthesis conditions. However, exposing two surface plasmon resonance bands, instead of one, could be due to the aggregated particles, which may

(39) Venkov, Tz.; Hess, C.; Jentoft, F. *Langmuir* **2007**, *23*, 1768.

(40) Hotchkiss, J. W.; Lowe, A. B.; Boyes, S. G. *Chem. Mater.* **2007**, *19*, 6.

(41) Milenkovic, S.; Nakayama, T.; Rohwerder, M.; Hassel, A. W. *J. Cryst. Growth* **2008**, *311*, 194.

have coupled plasmon bands at different wavelengths, and/or to the anisotropic shapes disparate from either spheres or wires in each sample.

3.4. Catalytic Performances of WGSR on Au Nanowire and Au Nanoparticle/FSM-16. The WGS reaction ($CO + H_2O \rightarrow CO_2 + H_2$) was performed at reduced pressure (P_{CO} = 60 torr, P_{H_2O} = 5 torr) for both samples at 323 K. As shown in Figure 7, Au nanowires encapsulated in FSM-16 exhibited higher activity in WGSR (~3 times), forming an equimolar mixture of CO_2 and H_2 than that on Au nanoparticles/FSM-16. Performing the same reaction on a pretreated nanowire sample (submitted into H_2; 10 torr, at 623 K for 3 h) at 323 K destroyed the activity, proposing that this deactivation is caused by forming big metallic Au particles (sintering) together with the induced changes on Au speciation. It can be stated that the strength of the CO cluster bonds depend on the environment of the atom that the CO interacts with; thus, the restructuring of nanowires following reduction at 623 K was expected to restrict the Brownian motion of CO along the deformed nanowires[42] and, most likely, their cohesive energy (Figure 7). In this figure, it can be seen that the catalyst activity was initially low (induction period) and then gradually increased, as the Au^+ of tiny nanoparticles is converted to Au^0 that proposed to be the active sites.

The strength of the CO cluster bonds depends on the environment of the atom that the CO interacts with. Thus, in the presence of water, represented by the band at 1640 cm^{-1} (not shown), an expected facile breaking of the chlorine bridges of Au_2Cl_6 is expected[32] upon raising the temperature to 338 K. This is supported by decreasing the intensity of the former IR band while raising the temperature from 323 to 338 K. Furthermore, restructuring of wires at 338 K is expected as well, thus restricting the Brownian motion of CO along the deformed nanowires,[42] causing all together an induction period responsible for HCl evolution and OH groups formation.

Discussing the activity of the WGSR in terms of decreasing Au dispersion (as deduced from XRD and TEM) highlights that this reaction is a structure-sensitive (morphology) one. Characterization of AuFS using XRD, UV−vis diffuse reflectance, and FTIR CO adsorption shows that Au nanowires acquire electron deficiency on their surfaces as well as decreased particles size; as deduced from XRD and TEM investigations, which together activate the surface reaction of WGS on the Au nanowires, comparatively. Electron deficiency of Au nanowires can enhance the nucleophilic attack of H_2O to CO adsorbed on AuFSwire, where the back bonding from Au to CO is weaker and thus enhances, comparatively, the WGSR activity.

To further investigate the gold morphology effect, the Au nanowires sample submitted to WGS following reduction at 623 K for 3 h was investigated by TEM (Figure 8). The TEM micrograph shows the presence of some gold patches distributed not periodically inside the pore system and rather showed larger particles (130−150 nm size) with mean diameter of 53 nm as well as agglomeration of some others, probably deposited on the external surface of the support. The external particles seen in this figure were detected by XRD (not shown) and indeed belong to the Au^0 phase. The activity data seem to support our point of view that as accumulation of Au nanoparticles (Au^0) increases together

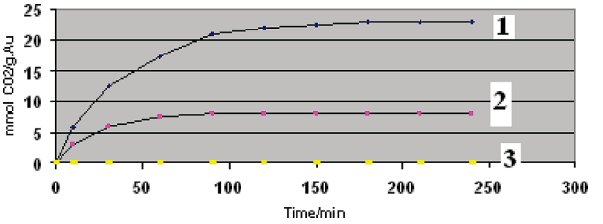

Figure 7. Effect of Au shape encapsulated in FSM-16 on the activity toward the WGSR at 323 K. Reaction conditions; 5 wt % Au loading, 0.1 g of catalyst, P_{CO} = 60 torr, P_{H_2O} = 5 torr: (1) AuFSwire, (2) AuFSpart, (3) AuFSwire submitted to H_2 reduction at 673 for 3 h.

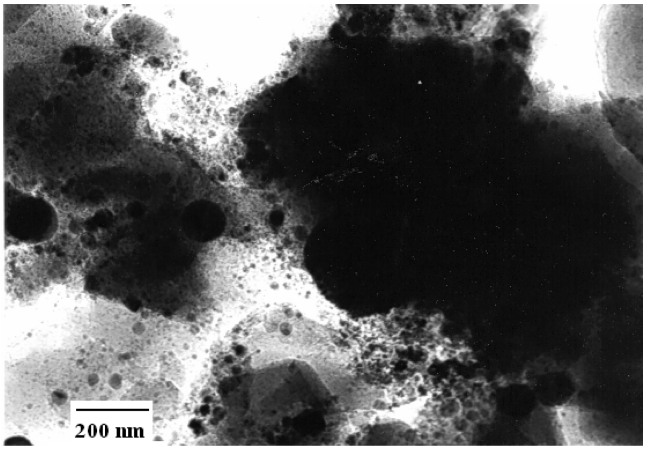

Figure 8. TEM image of AuFSwire following submission into H_2 reduction at 673 K for 3 h.

with growing particles size, a pronounced loss of activity is attained eliminating the overall WGS activity. Generally, a committed change on geometries could lead to a variation of defects, which could be active sites for CO oxidation and WGSR [43] as well as the nature of defects on Au nanoparticles (wires).

The existence of aggregates of circular particles besides those of nanowires, Figure 1, could lead to the suggestion of the bifunctional activity. One cannot deny that Au nanoparticles can play a role in activity, since AuFSpart presented some activity; however, when it loses dispersion and form big particles of Au^0, they become inaccessible, as depicted in Figure 8. Therefore, from what has been presented, Au^0 species including both nanowires and small aggregates (metallic nanoparticles; see Figure 1) contribute significantly, if not predominantly, to WGS activity and can not be considered spectator species.

Increasing the CO stretching frequency on Au nanoparticles (2088, 2079, and 2069 cm^{-1}) more than on the corresponding ones on Au nanowires might give a hint on increasing the adsorption energy on the former comparatively. However, the committed decrease in activity on the big nanoparticles might be associated with the size of the clusters formed, that is, CO adsorption energy deceases significantly as the size of the clusters is increased.[42] In addition, binding CO molecules on the above-mentioned bridge positions (Au−CO−Au) might restrict the mobility of

(42) Oncel, N.; Van Beek, W. J.; Huijben, J.; Poelsema, B.; Zandvliet, H. J. W. *Surf. Sci.* **2006**, *600* (2), 4690.

(43) Hashmi, S. K.; Hutchings, G. J. *Angew. Chem., Int. Ed.* **2006**, *45*, 7896.

CO in a sense that long hopping distance for diffusion along the Au nanoparticles to properly interact is forbidden probably for increasing the binding energy. Binding CO at the bridge positions of the Au diamers on the Au nanowires, of lower binding energy, might let CO move easier and closer to the surface to further interact with water. In addition, geometric constructions of possible atomic arrangements are suggested for nanowires[44] and thus acquire defects on their surfaces that might play another crucial role in catalyzing WGSR.

The facile interaction affirmed for AuFSwire upon interaction with CO and the presence of stabilized species of Au^{+} and Au^{3+} rather than with AuFSpart indicates that the interaction with CO for both samples follows different mechanisms. Specifically, performing WGS activity on Au catalysts at such low temperatures (323 K) led us to assume that an associative mechanism rather than a regenerative one is operated[38,42] in the sense of forming an active formate (carbonate) intermediates through participating CO, that attached to metal, with either OH groups, of the support, or with OH, of water molecules.

(44) Ge, Q.; Song, C.; Wang, L. *Comput. Mater. Sci.* **2006**, *35* (3), 247.

Conclusion

In this work, a procedure involving γ-ray to fabricate free-standing Au nanowires encapsulated inside FSM-16 have been demonstrated and evaluated for WGSR in comparison with Au nanoparticles. The low temperature (323 K) WGS activity on the former was higher (3 times) than that on the latter. This enhanced activity was primarily depended on the Au^{0} moieties, including both nanowires and small aggregated metallic nanoparticles. Nevertheless, the interaction of the wires with the internal surface of the template plays a unique role too as it reveals an enhancement in the electronic deficiency of the wires and rather modifies their dispersions, as revealed from XRD. TEM and XRD analyses revealed that the deactivation of Au nanowires (small nanoparticles) was correlated with sintering of Au moieties, following reduction, as well as consequent changes in shape from wire to rounded crystallites, those actually affected the nature of active centers.